International Journal of Minerals, Metallurgy and Materials
Volume 17, Number 4, August 2010, Page 481
DOI: 10.1007/s12613-010-0345-1

Microstructural evolution of titanium matrix composite coatings reinforced by *in situ* synthesized TiB and TiC by laser cladding

Jun Li, Zhi-shui Yu, Hui-ping Wang, and Man-ping Li

School of Materials Engineering, Shanghai University of Engineering Science, Shanghai 201620, China
(Received: 22 August 2009; revised: 5 October 2009; accepted: 13 October 2009)

Abstract: Titanium-based composite coatings reinforced by *in situ* synthesized TiB and TiC particles were successfully fabricated on Ti6Al4V by laser cladding using Ti-B_4C-Al or Ti-B_4C-C-Al powders as the precursor materials. The microstructural and metallographic analyses were made by X-ray diffraction (XRD), optical microscope (OM), scanning electron microscopy (SEM), and electron probe microanalysis (EPMA). The results show that the coatings are mainly composed of α-Ti cellular dendrites and a eutectic transformation product in which a large number of coarse and fine needle-shaped TiB and a few equiaxial TiC particles are homogeneously embedded. A thin dilution zone with a thickness of about 100 μm is present at the interface, and it consists of a few TiB and TiC reinforcements and a large number of lamella grains growing parallel to the heat flux direction in which a thin needle-shaped microstructure exists due to the martensitic transformation. The microstructural evolution can be divided into four stages: precipitation and growth of primary β-Ti phase, formation of the binary eutecticum β-Ti+TiB, formation of the ternary eutecticum β-Ti+TiB+TiC, and solid transformation from β-Ti to α-Ti.

Keywords: coating; laser cladding; *in-situ* synthesis; microstructure

[*This work was financially supported by the Shanghai Science and Technology Development Foundation (No.08QA14035), the Special Foundation of Shanghai Education Commission for Nano-Materials Research (No.0852nm01400), and the Crucial Project of Shanghai Science and Technology Commission (No.08520513400).*]

1. Introduction

Titanium alloys are widely used in aerospace, chemical, petrochemical, and marine industries as key structural components due to their combination of high strength-to-weight ratio, excellent corrosion resistance, and elevated-temperature mechanical properties [1]. However, owing to their poor resistance to sliding wear, their potential applications as substitutes for tribological components are restricted [2]. Wear is essentially a surface-dependent property that may be improved by appropriately tailoring the surface microstructure and/or composition, namely, surface modification without affecting the bulk [3]. In recent years, the laser cladding of ceramic-metal composite coatings onto Ti-alloy substrates has been used to improve the surface properties of titanium alloys. Ceramic phases, such as TiN [4], TiC [5], Ti_3Al [6], TiB [7], and Ti_2Ni_3Si [8], have been *in situ* synthesized during laser cladding. Among *in situ* synthesized reinforcements, TiB and TiC are regarded as the two best reinforcements in a titanium matrix due to their high elastic modulus, similar density to Ti alloys, and excellent interfacial bonding with titanium matrices [9]. Unfortunately, *in situ* synthesized TiB-TiC reinforced titanium matrix composites were fabricated as bulk materials by the ingot metallurgy technique (IM) [10], self-propagation high-temperature synthesis (SHS) [11], or powder metallurgy (PM) [12], *etc.*, which are rather complex and may result in material waste and increased costs. There are few reports about the preparation of titanium matrix composite coatings reinforced by *in situ* synthesized TiB and TiC on titanium alloys by laser cladding at present [13]. The current limited studies mainly focus on microstructural characteri-

Corresponding author: Jun Li E-mail: jacob_lijun@sina.com

zations and have little detailed discussion about the microstructural evolution of the coating or the interface.

The aim of the present work was to *in situ* synthesize TiC-TiB reinforced titanium matrix composite coatings on Ti6Al4V substrates by laser cladding. An investigation concerning the microstructure and phase was carried out. Based on this investigation, the possible mechanism of microstructural evolution of the TiB and TiC reinforcements is discussed in detail, which will contribute to acquire the desirable microstructure by rationally controlling the chemical composition of the cladding material and further endow the laser coating with more excellent mechanical properties.

2. Experimental

A Ti6Al4V alloy with a composition of 6.5wt% Al, 4.26wt% V, and the balance of Ti was used as a substrate material. It was hot rolled and annealed in the α+β range and was machined into cylinders of 50 mm in diameter and 10 mm in length. The substrate surface was polished with 200-grit SiC abrasive paper and degreased in acetone prior to coating. The chemical compositions of the powder mixtures used for the synthesis of composite coatings are shown in Table 1. The powder mixtures were mixed with a binder (polyvinyl alcohol, 4 g per 100 mL H_2O) to form a slurry and then preplaced on the substrate to form a layer of 1.0 mm in thickness. The substrate with the preplaced layer was dried at 90°C for 5 h.

Table 1. Chemical composition of the powder mixtures used for the synthesis of composite coatings wt%

Sample	Ti	B_4C	C	Al
1	87	9	0	4
2	86	9	1	4
3	85	9	2	4

Laser cladding was carried out using a 5-kW CO_2 laser with an applied power (P) of 3.5 kW and a beam diameter (D) of 4 mm at a scanning speed (v) of 5 mm/s. The laser parameters had been optimized to ensure a good interface fusion, a smooth coating surface, and a minimum dilution. The molten pool was shielded by blowing high-pressure nitrogen gas over the surface to prevent heavy oxidation during laser treatment.

Phase constituents of the coatings were analyzed by a Rigaku D/mas 2550 V X-ray diffractometer (XRD) with Cu K_α radiation. The microstructural characterization was carried out by means of a VHX-600K optical microscope (OM), a JSM6460 scanning electron microscope (SEM), and an INCN electron probe microanalyzer (EPMA). The cross-section of the samples for microstructure observations was prepared on a Buehler Phoenix 4000 sample preparation system and then rinsed with alcohol and acetone. A mixture consisting of 20vol% HF and 80vol% HNO_3 was used as the etchant.

3. Results and discussion

3.1. XRD analyses

Phase constituents of samples 1 and 3 are identified from X-ray diffraction spectra shown in Fig. 1. According to the indexed results of the diffraction peaks in terms of the JCPDS standard cards no.44-1294 for α-Ti, no.05-0700 for TiB, and no.02-1179 for TiC (as shown in Table 2), the coatings mainly include a great amount of α-Ti as the matrix in which a certain amount of elements, such as Al and C, are dissolved and a few of TiB and TiC as the reinforcements. The XRD spectrum of sample 1 is very similar to that of sample 3 except a little difference in the peak intensities of TiC phase, namely, they are increased when a small amount of C is added into the coatings. It can be concluded that the addition of C will contribute to the formation of TiC. A few diffraction peaks are not indexed due to the possible formation of other compounds in the Ti-B_4C-Al or T-B_4C-C-Al system. Usually, it is very difficult to identify the present phases in the coating. One reason is that the interplanar distances corresponding to the diffraction peaks of possible phases in the coating are close to each other. Another important reason may be the nonequilibrium effects of rapid melting and solidification in laser cladding, which may result in an extension of saturation and distortion of the lattices [14]. TiB and TiC are new phases that were *in situ* synthesized among Ti, B_4C, and C in the coatings during laser cladding. No B_4C and C phases are observed, which means that the reactions among Ti, B_4C, and C consumed all of the preplaced B_4C and C powders. The following reactions among Ti, B_4C, and C may take place.

$$5Ti+B_4C=4TiB+TiC \quad (1)$$

$$3Ti+B_4C=2TiB_2+TiC \quad (2)$$

$$Ti+C=TiC \quad (3)$$

The changes in Gibbs free energy of the above reactions were calculated using thermodynamic data from Ref. [15]. As shown in Fig. 2, the $\Delta G^\ominus$ of the three reactions is negative up to 2500 K, which indicates that the three reactions can spontaneously occur, namely, TiB_2, TiB, and TiC can be formed in the coatings. With the increase in tem-

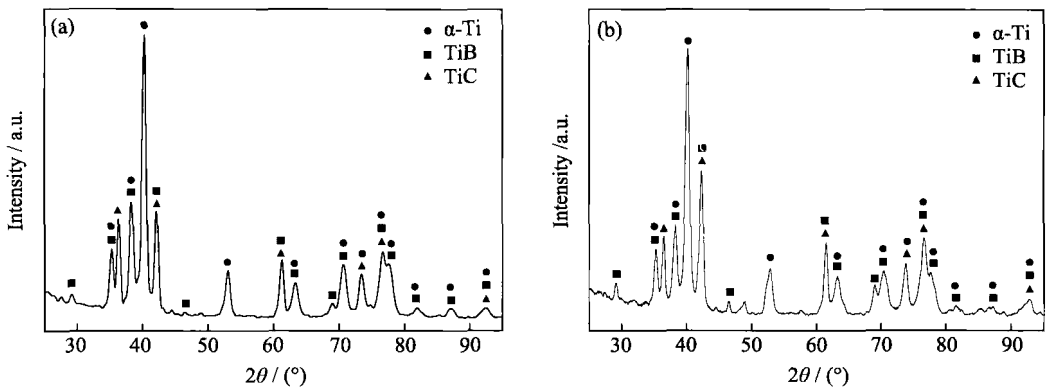

Fig. 1. XRD diagrams for samples 1 (a) and 3 (b).

Table 2. XRD data for samples 1 and 3, standard α-Ti (JCPDS card no.44-1294), TiB (JCPDS card no.05-0700), and TiC (JCPDS card no.02-1179)

Sample	Experimental data		α-Ti (JCPDS card no.44-1294)		TiB (JCPDS card no.05-0700)		TiC (JCPDS card no.02-1179	
	2θ / (°)	d / nm	d / nm	I/I_1	d / nm	I/I_1	d / nm	I/I_1
1	29.178	0.30581	—	—	0.30530	32	—	—
3	29.178	0.30581						
1	35.260	0.25433	0.25550	25	0.25430	80	—	—
3	35.240	0.25447						
1	36.399	0.24662	—	—	—	—	0.24700	80
3	36.460	0.24623						
1	38.259	0.23505	0.23410	30	0.23460	80	—	—
3	38.361	0.23445						
1	40.280	0.22371	0.22430	100	—	—	—	—
3	40.200	0.22414						
1	42.140	0.21426	—	—	0.21400	100	0.21500	100
3	42.319	0.21339						
1	46.503	0.19512	—	—	0.19560	40	—	—
3	46.519	0.19506						
1	53.140	0.17221	0.17262	13	—	—	—	—
3	52.979	0.17270						
1	61.261	0.15118	—	—	0.15280	32	0.15200	100
3	61.580	0.15048						
1	63.361	0.14667	0.14753	11	0.14610	28	—	—
3	63.381	0.14663						
1	69.040	0.13592	—	—	0.13620	72	—	—
3	68.999	0.13600						
1	70.699	0.13314	0.13320	11	0.13310	24	—	—
3	70.320	0.13376						
1	73.479	0.12877	0.12776	1	—	—	0.13000	80
3	73.800	0.12829						
1	76.660	0.12420	0.12481	9	0.12440	40	0.12400	60
3	76.580	0.12431						
1	77.580	0.12296	1.2324	6	1.2190	16	—	—
3	77.679	0.12282						
1	81.980	0.11743	1.1707	1	1.1810	28	—	—
3	81.641	0.11784						
1	87.023	0.11188	1.1215	1	1.1010	16	—	—
3	88.815	0.11008						
1	92.359	0.10676	1.0643	1	1.0790	24	1.0800	40
3	93.056	0.10614						

Note: θ—diffraction angle; d—Interplanar spacing; I/I_1—relative intensity.

perature, the $\Delta G^{\ominus}$ gets more positive, indicating that the spontaneous trends of these reactions are gradually decreased. At the same temperature, spontaneous chemical reactions follow the order: (1)>(2)>(3). That is to say, TiB can be formed in preference to TiB_2, so the *in situ* synthesis of TiB and TiC in the Ti-B_4C or Ti-B_4C-C system is liable to take place. However, no TiB_2 is observed based on the XRD analysis results, which should be attributed to the excess of titanium in the used systems. *In situ* synthesized TiB_2 will simultaneously react with the titanium matrix by the following reaction.

$$Ti+TiB_2=2TiB \quad (4)$$

As shown in Fig. 2, the thermodynamic calculation result reveals that this reaction can also spontaneously occur.

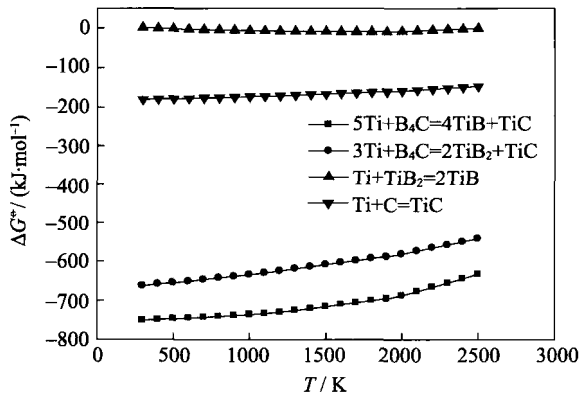

Fig. 2. Changes in Gibbs free energy as a function of temperature for Eqs. (1)-(4).

3.2. Microstructural characterization

An overview with the SEM of TiB+TiC/Ti composite coatings is depicted in Fig. 3, clearly revealing the microstructure of the coatings involving the morphologies of TiB and TiC phases. The microstructure of the coatings is very uniform and is mainly composed of coarse primary cellular dendrites (C1), coarse needle-shaped particles (C2), a few fine needle-shaped particles (C3), and equiaxial particles (C4). Clearly, the coarse primary cellular dendrites should be α-Ti, and particles with different morphologies are reinforcements that may be TiB or TiC. To further identify the phase constituents of these particles with different morphologies, elemental analysis was carried out at different zones labeled in Figs. 3(b) and (c), and the corresponding results are given in Fig. 4 and Table 3. The coarse/fine needle-shaped particles only consist of Ti and B, and the atom ratio of Ti to B is approximately 1:1; the fine equiaxial particles only consist of Ti and C, and the atom ratio of Ti to C is about 1.4:1. Combining with the XRD analyses, it can be inferred that they should be TiB and TiC, respectively. TiC and fine needle-shaped TiB particles distribute within the interdendritic zone. For coarse TiB particles, one part is located within the interdendritic zone, and another part is surrounded by coarse cellular dendrites. With the increase of C content, the number and the size of coarse TiB particles decrease gradually. The difference in morphologies between TiB and TiC can be mainly related with their difference in crystal structures. TiC has a B1 crystal structure, the unit cell is completely symmetrical without a preferential growth crystal facet no matter what geometric configuration and chemical bond are, which makes TiC grow in equiaxed or near-equiaxed shape when TiC is precipitated by the eutectic reaction [16]. TiB has a B27 prismatic structure and grows preferably along the [010] crystal direction for the distribution of atoms and chemical bonds is asymmetrical [17]. On the other hand, the concrete difference in morphologyies for reinforcements can also be rationalized by the microstructural evolution progress. The growth mechanism of reinforcements can be divided into the diffusion mechanism and the dissolution precipitation mechanism according to the processing temperature. When the temperature is lower than that related with the liquid phase line, reinforcements are *in situ* synthesized by the diffusion mechanism; on the contrary, the dissolution precipitation mechanism plays a key role in the formation of reinforcements. In this research, the heat exerted on the molten pool is comparatively high due to the high laser power of 3.5 kW; furthermore, reactions (1) and (2) will release a great amount of heat, which has been confirmed by many researchers [17-18]. The overlap of two parts of heat will result in a drastic enhancement in temperature and make *in situ* synthesized TiB and TiC melt in the liquid titanium during fabrication. During the subsequent cooling, TiB and TiC will nucleate and grow from the liquid phase. According to the projection of liquidus surfaces in the Ti-B-C ternary phase diagram [19] shown in Fig. 5, the compositions of the used powder mixtures are located at the rich-titanium corner, in which a ternary eutectic reaction $L \rightleftharpoons$ β-Ti+TiB+TiC and three binary eutectic reactions corresponding to $L \rightleftharpoons$ β-Ti+TiB, $L \rightleftharpoons$ β-Ti+TiC, and $L \rightleftharpoons$ TiB+TiC are present. Combining with the analysis of the Ti-B-C phase diagram and the observation of the coating microstructure, the microstructural evolution process can be described as follows.

(1) Precipitation of primary phase β-Ti. TiB and TiC are *in situ* synthesized and melted in the liquid phase as analyzed in the former. In the subsequent cooling process, pri-

mary phase β-Ti will nucleate from the liquid phase by the reaction of $L \rightleftharpoons \beta\text{-}Ti_p + L_p$ (subscript p represents the primary phase) and grow into the coarse cellular or dendritic shape due to the sufficient time and space to grow in the liquid alloy.

(2) Formation of the binary eutectic of β-Ti and TiB. As the temperature gradually reduces, one part of the liquid phase is further transformed into β-Ti and TiB by the binary reaction $L_p \rightleftharpoons (\beta\text{-}Ti + TiB)_e + L_e$ (subscript e represents the eutectic phase). β-Ti and TiB will grow quickly due to the rapid atom diffusion in the liquid phase. β-Ti may collide with TiB growing preferably along the [010] crystal direction and will grow around the surface of needle-shaped TiB. As a result, one part of coarse needle-shaped TiB particles are surrounded by β-Ti, as shown in Fig. 3(b). With the increase of C content, the temperature at which the binary eutectic reaction begins to occur is decreased. The reaction temperature range and time for this reaction will be shortened to a certain extent. As a result, the number and the size of the binary eutectic product TiB are reduced.

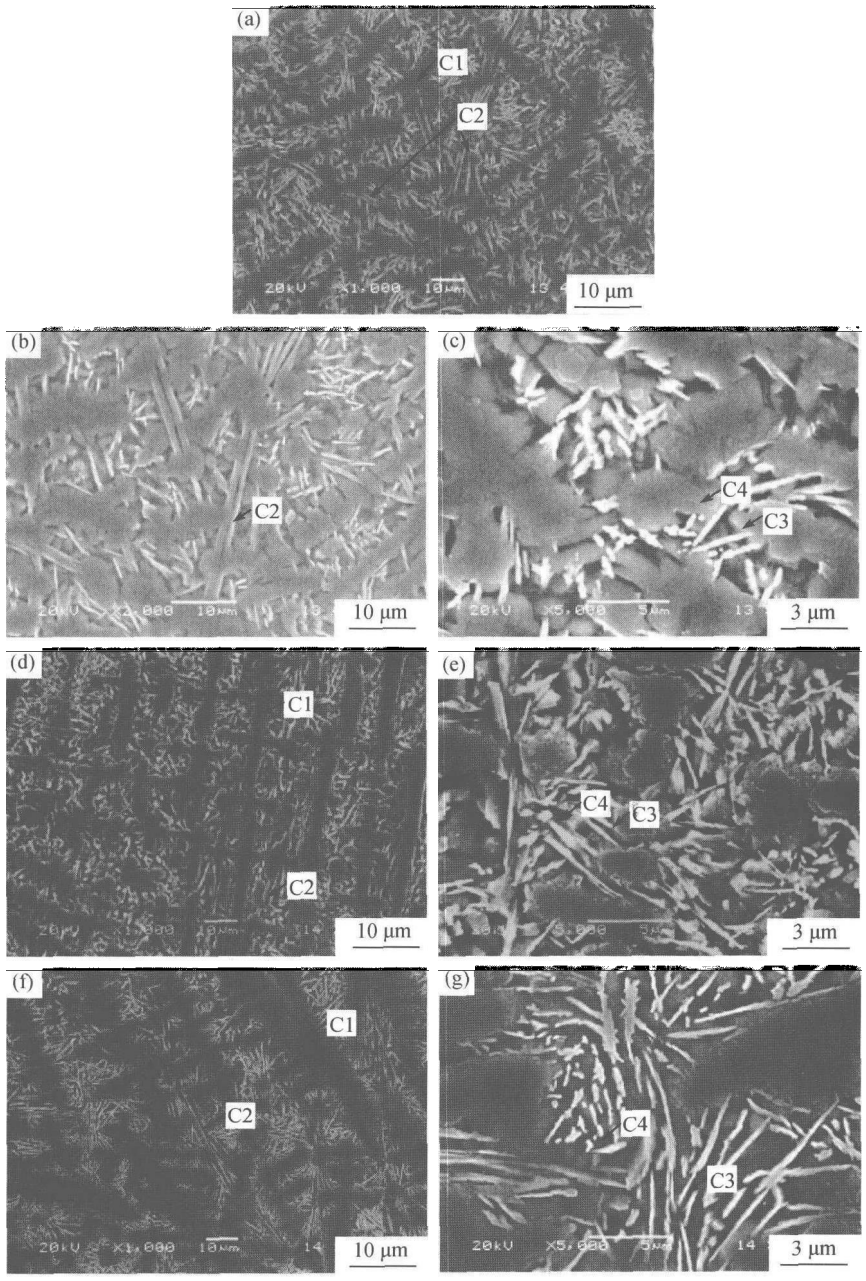

Fig. 3. SEM images from the cross-section of the coatings: (a), (b), and (c) microstructures of samples 1; (d) and (e) microstructures of sample 2; (f) and (g) microstructures of sample 3.

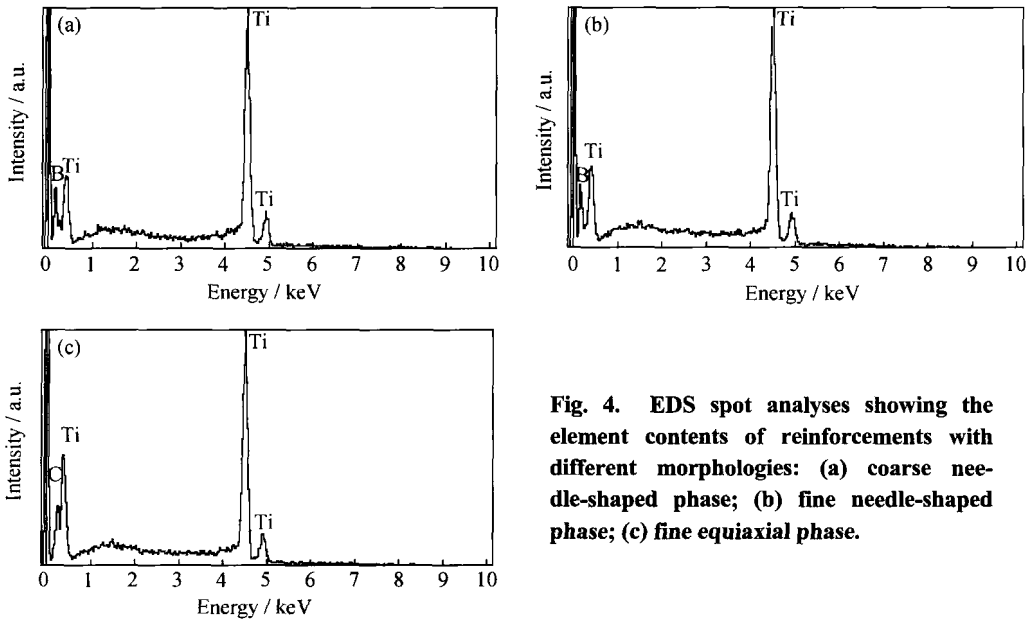

Fig. 4. EDS spot analyses showing the element contents of reinforcements with different morphologies: (a) coarse needle-shaped phase; (b) fine needle-shaped phase; (c) fine equiaxial phase.

(3) Formation of the ternary eutectic of β-Ti, TiB, and TiC. With a further decrease in temperature, the remaining liquid phase will be crystallized into three kinds of phases corresponding to β-Ti, fine needle-shaped TiB, and equiaxial TiC particles by the ternary eutectic reaction $L_e \rightleftharpoons (\beta\text{-Ti+TiB+TiC})_e$. Fine needle-shaped TiB and equiaxial TiC particles are homogeneously embedded in the matrix. Owing to the fast reaction time and slow atom diffusion rate in the solid, TiB and TiC are very fine in comparison with primary β-Ti and the binary eutectic product TiB.

(4) Formation of α-Ti. β-Ti will be transformed into α-Ti by the allotropic transformation reaction β-Ti ⇌ α-Ti soon after. Then, α-Ti, TiB, and TiC are maintained at room temperature.

The morphology of the interface between sample 1 and the substrate is shown in Fig. 6(a). The interface is very

Table 3. Chemical composition of the zones indicated by the arrows in Figs. 3(b) and (c) **at%**

Zone	Ti	B	C
C2	54.14	45.86	—
C3	53.32	46.68	—
C4	59.25	—	40.75

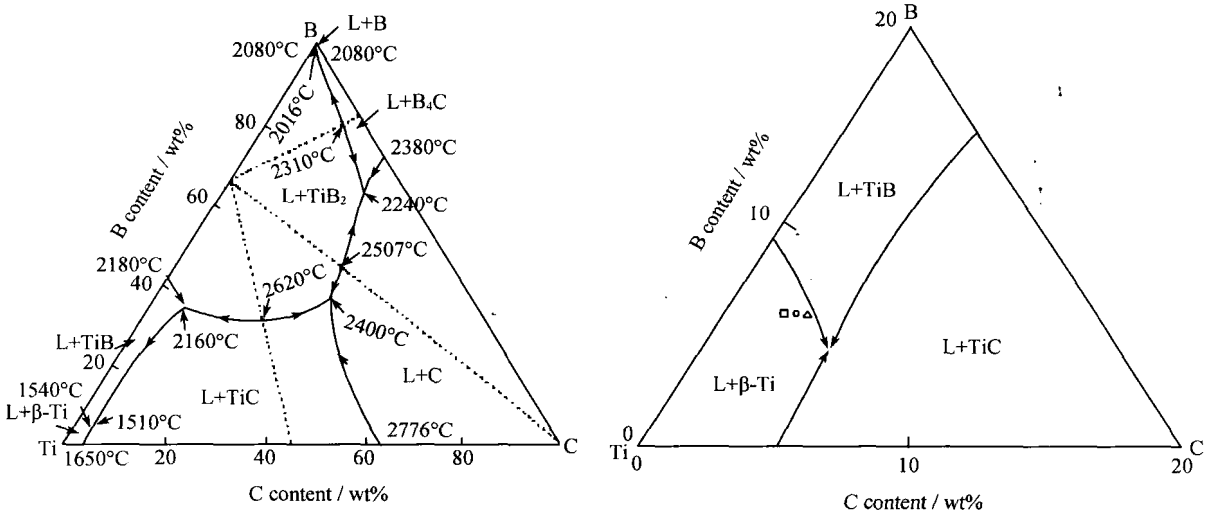

Fig. 5. Projection of liquidus surfaces in the Ti-B-C phase diagram (a) and zone at the rich-titanium corner (b) (□—composition points of sample 1; ○—composition points of sample 2; Δ—composition points of sample 3).

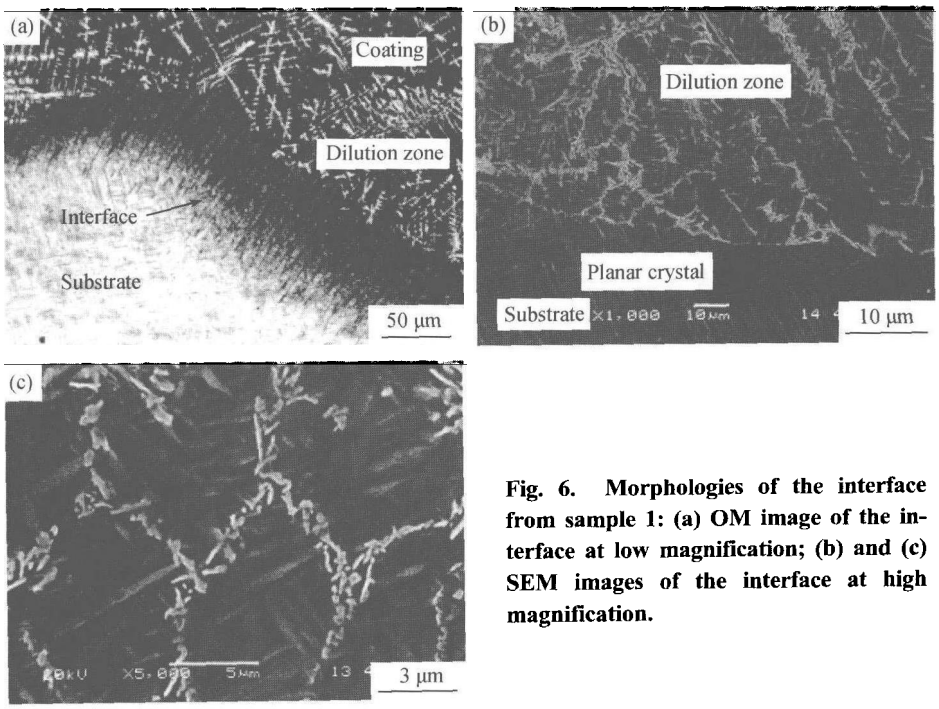

Fig. 6. Morphologies of the interface from sample 1: (a) OM image of the interface at low magnification; (b) and (c) SEM images of the interface at high magnification.

clear and continuous, no cracks, pores, delamination, or other inclusions are observed at the interface region. A dilution zone with a thickness of about 100 μm is present at the interface and consists of a large number of lamella phases growing perpendicular to the substrate, which will reduce the difference in hardness and expandability between the coating and the substrate and will further contribute to forming an excellent metallurgical bond between them. Two more detailed SEM images are shown in Figs. 6(b) and (c). A thin layer of planar crystal with a thickness of 1 μm is found at the interface, and there are a few fine reinforcements at the boundaries of lamella phases and a great number of fine needle-shaped grains within the lamella phase. It is well known that the microstructure characteristics of the interface mainly depend on the parameter of G/R (G and R represent the temperature gradient and solidification rate, respectively) reported in Ref. [14], and the ratio of G/R at the interface is very high (the solidification rate is initially zero at the interface). Therefore, the solidification starts from the surface of the substrate by epitaxial growth on the substrate without nucleation and a plane proceeds along the surface. As the solid/solution interface proceeds along the surface, the solidification structure switches successively to the lamella structure growing parallel to the heat flux direction due to the reduction in G/R. Subsequently, the eutectic microstructure in which TiB and TiC are embedded is formed along the lamella grain boundaries. At last, a thin needle-shaped microstructure is formed by a martensitic transformation in lamella grains owing to the very rapid solidification rate.

4. Conclusions

(1) Titanium matrix composite coatings reinforced by *in situ* synthesized TiB-TiC have been successfully fabricated on Ti6Al4V by laser cladding. The coatings are mainly composed of α-Ti cellular dendrites and a eutectic transformation product in which a large number of coarse and fine needle-shaped TiB particles and a few equiaxial particles are homogeneously embedded. A thin dilution zone with a thickness of about 100 μm is present and consists of a few TiB and TiC reinforcements and a large number of lamella grains in which a thin needle-shaped microstructure exists by a martensitic transformation.

(2) The microstructural evolution can be divided into four stages: $L \rightleftharpoons \beta\text{-Ti}_p + L_p$; $L_p \rightleftharpoons (\beta\text{-Ti}+\text{TiB})_e + L_e$; $L_e \rightleftharpoons (\beta\text{-Ti}+\text{TiB}+\text{TiC})_e$; and $\beta\text{-Ti} \rightleftharpoons \alpha\text{-Ti}$.

References

[1] Y. Wang and H.M. Wang, Wear resistance of laser clad Ti_2Ni_3Si reinforced intermetallic composite coatings on titanium alloy, *Appl. Surf. Sci.*, 229(2004), p.81.

[2] R.L. Sun, D.Z. Yang, L.X Guo, and S.L. Dong, Laser cladding of Ti-6Al-4V alloy with TiC and TiC+NiCrBSi powders, *Surf. Coat. Technol.*, 135(2001), p.307.

[3] M. Hazra, A.K. Mondal, S. Kumar, *et al.*, Laser surface clad-

ding of MRI 153M magnesium alloy with (Al+Al_2O_3), *Surf. Coat. Technol.*, 203(2009), p.2292.

[4] B.G. Guo, J.S. Zhou, S.T. Zhang, *et al.*, Microstructure and tribological properties of *in situ* synthesized TiC, TiN, and SiC reinforced Ti_3Al intermetallic matrix composite coatings on pure Ti by laser cladding, *Mater. Sci. Eng. A*, 480(2008), p.404.

[5] H.C. Man, S. Zhang, F.T. Cheng, and T.M. Yue, Microstructure and formation mechanism of *in situ* synthesized TiC/Ti surface MMC on Ti-6Al-4V by laser cladding, *Scripta Mater.*, 44(2001), p.2801.

[6] B.G. Guo, J.S. Zhou, S.T. Zhang, *et al.*, Phase composition and tribological properties of Ti-Al coatings produced on pure Ti by laser cladding, *Appl. Surf. Sci.*, 253(2007), p.9301.

[7] R. Banerjee, A. Genc, D. Hill, *et al.*, Nanoscale TiB precipitates in laser deposited Ti-matrix composites, *Scripta Mater.*, 53(2005), p.1433.

[8] Y. Wang and H.M. Wang, Wear resistance of laser clad Ti_2Ni_3Si reinforced intermetallic composite coatings on titanium alloy, *Appl. Surf. Sci.*, 229(2004), p.81.

[9] D. Hill, R. Banerjee, D. Huber, *et al.*, Formation of equiaxed alpha in TiB reinforced Ti alloy composites, *Scripta Mater.*, 52(2005), p.387.

[10] Y. Liu, L.F. Chen, H.P. Tang, *et al.*, Design of powder metallurgy titanium alloys and composites, *Mater. Sci. Eng. A*, 418(2006), p.25.

[11] M.J. Mas-Guindal, L. Contreras, and X. Turrillas, Self-propagating high-temperature synthesis of TiC-WC composite materials, *J. Alloys Compd.*, 419(2006), p.227.

[12] S. Gorsse, Y.L. Petitcorps, S. Matar, and F. Rebillat, Investigation of the Young's modulus of TiB needles *in situ* produced in titanium matrix composite, *Mater. Sci. Eng. A*, 340(2003), p.80.

[13] L.F. Cai, Y.Z. Zhang, and L.K. Shi, Microstructure and formation mechanism of titanium matrix composites coating on Ti-6A1-4V by laser cladding, *Rare Met.*, 26(2007), p.342.

[14] S. Yang, M.L. Zhong, and W.J. Liu, TiC particulate composite coating produced *in situ* by laser cladding, *Mater. Sci. Eng. A*, 343(2003), p.57.

[15] D.L. Ye, *Practical Inorganic Thermodynamics Manual*, Metallurgical Industry Press, Beijing, 2002, p.106.

[16] W.J. Lu, D. Zhang, X.N. Zhang, *et al.*, Microstructural characterization of TiC in *in situ* synthesized titanium matrix composites prepared by common casting technique, *J. Alloys Compd.*, 327(2001), p.248.

[17] X.N. Zhang, W.J. Lu, D. Zhang, and R.J. Wu, *In situ* technique for synthesizing (TiB+TiC)/Ti composites, *Scripta Mater.*, 41(1999), p.39.

[18] W.J. Lu, X.N. Zhang, D. Zhang, *et al.*, Thermodynamic research on *in situ* formation of TiB and TiC reinforced titanium matrix composites, *Chin. J. Nonferrous Met.*, 9(1999), p.220.

[19] H. Duschanek, P. Rogal, and H.L. Lukas, A critical assessment and thermodynamic calculation of the Boron-Carbon-Titanium (B-C-Ti) ternary system, *J. Phase Equilibria*, 16(1995), p.46.